Distribution and concentration of soluble manganese(II), soluble reactive Mn(III)-L, and particulate MnO_2 in the Northwest Atlantic Ocean

Matthew R. Jones[a]*, George W. Luther III[b], and Bradley M. Tebo[a]

[a] Division of Environmental and Biomolecular Systems, 3181 SW Sam Jackson Park Road, Portland, Oregon, 97239, USA.

[b] School of Marine Science and Policy, University of Delaware, 700 Pilottown Road, Lewes, Delaware, 19958, USA.

*corresponding author: matthew_r_jones@rocketmail.com

Abstract

As manganese cycles between its three oxidation states, encompassing soluble and particulate phases, it influences the biogeochemistry of organic carbon, nutrients, and many trace elements. However, measurements of manganese distributions and speciation in the open ocean have typically been based only on differentiating soluble (assumed to be manganese(II)) and particulate (assumed to be manganese(III,IV) oxides) forms. We measured particulate oxidized manganese (MnO_x, where $x \approx 1.8–2$), reactive soluble manganese(III) (soluble manganese(III) that forms a complex with desferrioxamine-B (Mn(III)-L_{DFOB})), and total dissolved manganese (dMn_T; manganese(II) + Mn(III)-L_{DFOB}) in Northwest Atlantic offshore waters (10–2600 m). Mn(III)-L_{DFOB} concentrations were from below the detection limit (0.008 nM) up to 0.76 nM and measured throughout the water column with higher concentrations near the base of the euphotic zone (~ 100 m), in the oxygen minimum zone (OMZ), and generally increasing from below the OMZ into the bottom waters. MnO_x ranged from 0.19 nM to 3.52 nM in the water column. Concentrations were high near the base of the euphotic zone where reactions of MnO_x with organic material are the likely source of the Mn(III)-L_{DFOB} observed there. Elevated MnO_x was also occasionally found in deep waters likely due to turbidity layers resulting from sediment resuspension. Mn(III)-L_{DFOB} accounted for up to 45% of the dMn_T and up to 74% of the total oxidized manganese (Mn(III)-L_{DFOB} + MnO_x) in different regions of the water column. Mn(III)-L_{DFOB} contributed 10–20% of the generally uniform total dissolved manganese concentration in the deep ocean. Both soluble and particulate oxidized forms of manganese (Mn(III)-L and MnO_x) are a significant component of the deep water manganese pool and likely play a prominent role in oceanic redox chemistry and organic carbon re-mineralization.

1.0 Introduction

Within the environment, particulate manganese(III,IV) oxide (MnO_x, where $x \approx 1.8–2$) is one of the strongest oxidants, yet our understanding of the behavior of manganese in aquatic systems is incomplete. The MnO_x/manganese(II) redox couple has a pivotal reactive intermediate oxidation state (manganese(III); Davies, 1969), through which most manganese-reducing and -oxidizing reactions occur (Luther, 1990). These redox reactions accompany reversible changes between insoluble and soluble forms. The recycling of MnO_x is the critical process in the manganese cycle as it directly impacts biogeochemical reactions. The MnO_x mineral has an efficient surface area that oxidizes organic carbon. While oxidizing organic material, MnO_x produces 10-times more low molecular weight organic acids than iron oxides (Chorover and Amistadi, 2001). During formation, MnO_x scavenges nutrients (Yao and Millero, 1996) and trace elements (Murray, 1975). Oxidation of organic carbon by MnO_x can break down high molecular weight material to low molecular weight compounds. Low molecular weight organics are more bioavailable (Søndergaard and Middelboe, 1995) and may lead directly to CO_2 formation through bacterial consumption (Sunda and Kieber, 1994) or they may be further oxidized to CO_2 abiotically (Chang Chien et al., 2009). The low molecular weight carbon concomitantly stabilizes manganese(III) in reactive organic complexes (Mn(III)-L; Jones et al., 2019b; Madison et al., 2013; Oldham et al., 2017a). Redox reactions occur below the euphotic zone and result in new MnO_x production and particle formation, which significantly enhances the oceanic sequestration of carbon (Boyd et al., 2019). Moreover, manganese oxides can intercalate up to 20% w/w organic carbon (Estes et al., 2017; Johnson et al., 2015).

The pivotal Mn(III)-L species is present in estuarine systems (Jones et al., 2019b; Oldham et al., 2017b, 2015), occurs at the suboxic/anoxic interfaces of sediments (Madison et al., 2013;

Oldham et al., 2019) and is found in variable but high concentrations in anoxic basins (Dellwig et al., 2012; Schnetger and Dellwig, 2012; Trouwborst et al., 2006). Manganese(III) is also present in open ocean waters (Jones et al., 2019a; Thibault de Chanvalon and Luther, 2019). However, because the methods to sensitively measure Mn(III)-L at sub-nanomolar concentrations have not, until recently, been available, there are no comprehensive measurements for open ocean waters. Here we apply two newly developed analytical techniques (Jones et al., 2019b, 2019a) for sensitive measurements of depth profiles of Mn(III)-L and MnO_x concentrations in the oxygenated waters of the Northwest Atlantic Ocean. We show that there are significant concentrations of Mn(III)-L in seawater and that this species is pervasive and persistent. We cannot yet propose the dominant formation pathway for Mn(III)-L because formation occurs following the oxidation of manganese(II) or reduction of manganese(IV). However, we propose that the presence of Mn(III)-L is an indicator of an active manganese cycle.

2.0 Methods

2.1 Locations and sampling

Offshore Atlantic locations (Fig. 1 and Table 1) in 2013, east from the Chesapeake Bay, and in 2014, east from Delaware Bay, were visited by the research vessel Hugh R Sharp. In 2013, three Conductivity-Temperature-Depth sensor profiles were cast. Station A1 (37 07.84 N, 073 19.72 W) sampled from 698 m to the surface, Station A2 (37 18.45 N, 073 23.79 W) sampled from 825 m to the surface, and at Station A2 (37 18.32 N, 073 24.03) there was an additional deep water sampling (2032 m). In 2014, two CTD casts were deployed. Station B1 (38 17.40 N, 072 43.70

W) sampled from 2602 m to the surface, and Station B2 (38 14.96 N, 072 45.27 W) sampled from 449 m to the surface. Continuous oxygen measurements were made during each cast.

All plastic ware, including sampling tubing (attached to the Niskin bottles), sampling bottles, centrifuge tubes, filter holders and syringes used for sampling were cleaned through two sequential washes: 3% micro90 detergent (1 week), 2.4 M AR grade HCl (1 week). Sampling bottles were stored containing 2.4 M trace-metal grade HCl. Between washes, sampling equipment was rinsed a minimum of three times with DI. During use, the polysulfone filter units were cleaned through brief multiple rinses (n = 3) of 1.2 M trace-metal grade HCl followed by DI. The 0.2 µm Whatman track etched polycarbonate filters were soaked in 1 M HCl for one week before rinsing in deionized water and storage in deionized water. Seawater samples were collected using a rosette system (12 × 12 L Niskin PVC bottles). For deployment, Niskin bottles were flushed with seawater as they remained open on descent during each cast. Samples were collected directly from the Niskin bottles into 500 mL polycarbonate bottles, being filled to the brim (625 mL) after filling and rinsing three times. Samples were stored in the dark at 4°C, and the whole sample filtered (625 mL through 45 mm × 0.2 µm Whatman Nuclepore track-etched polycarbonate membranes) within 20 min. All polysulfone filtration units and sample tubes were rinsed three times, either with the sample or filtrate, as required. Samples for soluble fractions of manganese were processed once the filtrate was available. The filters for the analysis of MnO_x were immediately processed, and the spectrophotometric analysis completed within 2–4 h.

2.2 Analytical

2.2.1 Particulate oxidized manganese [MnO_x]

The method to analyze the sample for MnO_x (Jones et al., 2019a) used the highly specific colorimetric probe leucoberbelin blue (LBB; Merck) (Altmann, 1972). This method has proven successful for measuring MnO_x in estuarine (Jones et al., 2019b; Oldham et al., 2015) and seawater samples (Jones et al., 2019b). Briefly, each filter membrane plus 2 mL of LBB reagent was placed in a 5 ml LDPE tube. The LBB reagent was 0.04% LBB in 1% Acetic acid (Merck) subsequently diluted 50-fold by 18.1 MΩ deionized water. The samples were occasionally agitated for 2–4 hours before measurement in a World Precision Incorporated (WPI) 100-cm liquid wave capillary cell (LWCC) connected through optical fiber cables to an Ocean Optics USB2000 spectrophotometer with a halogen light source (HL-200-FHSA). The absorbance at 624 nm corresponds to the blue-colored oxidized LBB maxima. If required, a baseline correction calculated from the slope of the linear regression between the absorbance at 480 and 700 nm was applied. The calibration standard was potassium permanganate. Strictly speaking, LBB measures the oxidizing equivalents of manganese and the computed MnO_x concentration derives from the oxidation state of +IV. Based on the LBB oxidation stoichiometry, if the MnO_x is computed as MnO_2 but contains 10% manganese(III) it introduces an error of -5% in the estimate of MnO_2. To account for the difference in the oxidation state of the manganese from the standard (permanganate, +VII) a factor of 2.5 was applied. The error on the LBB measurement was taken from the relative standard deviation of the standards (< 2%), as this was higher than the error on the repeat measurements of the sample. The analytical range for standards within the 100-cm LWCC was 10 to 400 nM and the limit of detection was 6.7 nM which, when corrected for the volume passed through the filter, was 0.022 nM.

2.2.2 Processing manganese(III) [Mn(III)-L] and total dissolved manganese [dMn_T] samples

Mn(III)-L was extracted and concentrated from 50 mL of the filtrate as a complex with the siderophore desferrioxamine-B [DFOB; Mn(III)-DFOB]. The added DFOB outcompetes the ambient ligands stabilizing reactive manganese(III) and weak-siderophore-complexed manganese(III). We operationally define this extracted fraction as Mn(III)-L_{DFOB} (Jones et al., 2019b). DFOB is a strong manganese(III) ligand (log K_{COND} = 13.2 in seawater (Luther et al., 2015); log $K_{[Mn(III)HDFOB+]}$ = 28.6 ± 0.5 in 0.1M NaCl (Duckworth and Sposito, 2005a)). The chromatographic extraction technique, coupled to a flow-injection analysis spectrophotometry quantification method successfully measured Mn(III)-L in estuarine and seawater samples (Jones et al., 2019b). Briefly, a small volume of recently prepared DFOB (mesylate salt, Merck) in deionized water was added to the 0.2 µm filtered seawater sample to a strength of 20 µM. The sample was left for 5–20 minutes before passing through inline chromatography cartridges containing an Oasis Hydrophilic-Lipophilic-Balanced (HLB; Waters) stationary phase (primed with 20 mM HEPES at pH 7.8) at 1 mL min^{-1}. The Mn(III)-DFOB complex that had concentrated on the solid-phase extraction column was eluted with 4 mL of methanol (12.5-fold concentration increase of the sample). The methanol was stored cold, -20°C, and on return to the laboratory, the Mn(III)-DFOB in the methanol was reduced through the addition of a small volume of 1.44 M hydroxylamine hydrochloride in deionized water that was added to a final concentration of 14.4 mM, the sample was then acidified to < pH 2 with 6 M nitric acid (HNO_3; Optima, Merck) for cold storage prior to analyses.

The samples for total dissolved manganese (dMn_T) analysis were retained in 15 mL pre-cleaned centrifuge tubes. Immediately after processing, a small volume of 1.44 M hydroxylamine hydrochloride in deionized water was added to a final concentration of 14.4 mM. Sample acidification for preservation, through the addition of 6 M nitric acid (4 µL per 1 mL sample),

occurred between two to four weeks later in the laboratory. The 2013 samples were stored for eight months before analysis and the 2014 samples for three months. Manganese stability issues affecting the concentration of soluble reduced manganese in the presence of acid plus a strong reductant within the storage time-frames are not likely an issue (Jensen et al., 2020; Stumm and Morgan, 1996). The estimated concentration of manganese(II) derived from the difference between the concentrations of dMn_T and Mn(III)-L_{DFOB}.

Processing of deionized water blanks commenced immediately the Mn(III)-L_{DFOB} and dMn_T sample processing had finished and the equipment rinsed. The deionized water blank was filtered as per the sample, spiked with DFOB and passed over the HLB columns. The methanol eluate is taken as the new Mn(III)-L_{DFOB} blank and processed as *per* a sample. After filtering deionized water and adding hydroxylamine hydrochloride, the acidification of the dMn_T blank occurred as *per* the sample. It is unlikely that seawater contains significantly high concentrations of strong ligands capable of complexing manganese(III). Moreover, seawater is unlikely to contain manganese species that are unreactive towards reduction by hydroxylamine hydrochloride (Thibault de Chanvalon and Luther, 2019). Therefore, the manganese speciation methods likely accounted for the majority of the available soluble manganese species.

2.2.3 Quantifying manganese(III) [Mn(III)-L] and total dissolved manganese [dMn_T] samples

We used Tiron flow injection analysis spectrophotometry (FIA-S) to measure manganese concentrations in the Mn(III)-DFOB in methanol and dMn_T seawater samples (Jones et al., 2019b). The method includes a chromatographic extraction phase using the Toyopearl AFChelate-650M stationary phase to remove the manganese from the methanol and the seawater

176 (Aguilar-Islas et al., 2006; Jones et al., 2019b; Milne et al., 2010). Isolation of the Mn(III)-DFOB
177 manganese from the methanol is required because, in a 100-cm LWCC, the direct measurement
178 of the Tiron semiquinone complex is affected by the absorbance of the methanol. In the presence
179 of H_2O_2, manganese catalyzes the oxidation of the sulfonated catechol Tiron to its semiquinone
180 form (Scharff and Genin, 1975). To quantify the manganese concentration, we
181 spectrophotometrically determined the absorbance at 424 nm, which corresponds to the
182 semiquinone complex that forms at pH > 9. The measurement of Mn(III)-DFOB (limit of
183 detection 0.008 nM using 1 mL and considering the 12.5-fold extraction protocol concentration
184 factor) and dMn_T (limit of detection 0.1 nM for 1 mL) as manganese(II) occurred on return to the
185 laboratory. The Tiron concentration during sample analysis was either 3.2 or 4 mM, and these
186 concentrations provide an analytical window < 0.24 to 10 nM, equivalent to a Mn(III)-L sample
187 range < 0.02 to 0.8 nM. The analyses of the National Research Council Canada SLEW-3
188 certified reference material (S_p ~ 15 and dMn_T = 29.5 ± 4 nM; salinity written as S_p as per the
189 Intergovernmental Oceanographic Commission Thermodynamic Equation of Seawater – 2010)
190 verified the method for manganese. Replicate analyses using FIA-S yielded total manganese
191 concentrations of 29.4 and 30.0 nM. Triplicate analyses of samples, standards or blanks were
192 within a relative standard deviation of < 2%.

193 **3.0 Results**

194 Physicochemical upper water (< 500 m) depth profiles vary between the four stations sampled in
195 2013 (A stations) and 2014 (B stations) from the North Atlantic Ocean off the central east coast
196 of the U.S. (Figs. 2 & 3). In 2013, the upper water structure of Station A2 extended
197 approximately 100 m deeper than Station A1 (Fig. 2), though Station A2 profiles were similar if
198 corrected by this depth difference. At Station A1 and A2, homogenous high salinity water (S_p >

35.6) extended from the surface to ~ 155 and 265 m, respectively, below which was the pycnocline, wherein salinity decreased to S_p = 35.0 by 400–500 m (Fig. 2). Near-surface waters were higher than 27°C and temperatures dropped rapidly to less than 17°C by 74 m. Following the steep temperature decrease over the upper thermocline was a more gradual decrease to 6–7°C by 400–500 m (base of the pycnocline). It is in the higher salinity water where the percentage oxygen saturation decreased towards its minimum (46% O_2 sat./126 µM). This minimum occurred in the pycnocline at 224 m and 324 m, Station A1 and A2, respectively (Fig. 2). The difference in surface salinity structure at Station A is likely related to the presence of warm-core rings and transient surface eddies (Evans et al., 1985; Joyce et al., 1983) affecting the depth profile of manganese (Bishop and Fleisher, 1987).

At Station B in 2014 (Fig. 3) the near-surface water salinity was 35.2 and salinity increased with depth to the maximum, S_p = 35.7. Due to sampling, and at Station B1 the salinity maximum was at 99 m whereas at Station B2 it was shallower at 36 m (Fig. 3). At the B Stations, the pycnocline was indicated by salinity decreasing with depth from the maxima to 35.07 by 450 m. Near-surface water temperatures were ~ 3°C lower in 2014 than in 2013, with an average of 24.2°C. The steepest observed thermocline occurred as the temperature dropped to 14.3°C by 97 m; the temperature continued decreasing to 6.8°C by 450 m. The temperature and salinity of Station B at 450 m were similar to Station A between 400–500 m. For the A and B stations at 400–500 m, salinity ranged from S_p = 35.05 to 35.08. As with Station A, the Station B percentage oxygen saturation minimum (46% O_2 sat./130 µM) occurred within the pycnocline; at Station B1 and B2, this minimum corresponded to a depth of 280 m.

In 2013, the surface water (~ 10 m) dMn_T was 10.8 ± 2.2 nM. In 2014, waters shallower than 40 m had 6.7 ± 0.7 nM dMn_T and the concentrations were slightly higher (< 1 nM) at 10 m

222 relative to ~ 40 m (Figs. 4 & 5). Station B had more samples taken in euphotic waters, and these
223 samples show a decrease of ~ 4 nM in dMn_T between 40 and 60 m; by ~ 95 m there was 2.2 ±
224 0.2 nM dMn_T. At Stations A1 and A2, below 70 m the average dMn_T was 3.6 ± 0.9 nM with a
225 maximum of 7.95 nM at 154 m (145 µM O_2). At the B stations, from 95 m down to the waters
226 influenced by the nepheloid layer (~ 2000 m), the average dMn_T was 1.7 ± 0.5 nM, and the
227 maximum was 2.7 nM at 371 m (151 µM O_2). The nepheloid layer (2602 m) contained 26 nM
228 dMn_T while there was elevated dMn_T (3.97 nM) at 2004 m.

229 The MnO_x oceanic profiles (Figs. 2 & 3) generally show low concentrations in the sunlit
230 surface waters due to photo-induced, organically-mediated reduction (Sunda et al., 1983) that
231 leads to high concentrations of dMn_T as manganese(II) (Figs. 4 & 5). There is high MnO_x (1.1 ±
232 0.4 nM) around the base of the euphotic zone (~ 100 m) with concentrations decreasing with
233 depth to the core of the oxygen minimum zone OMZ (0.4 ± 0.1 nM; 300–400 m). At Station A
234 (2013), through the oxygen minimum and into intermediate waters, MnO_x decreased slightly
235 with depth (Fig. 2). Station B (2014) profiles (Fig. 3) were more complex. At the lower limit of
236 the OMZ (448 m), MnO_x increased to 2.6 ± 0.4 nM, yet, below this region, the MnO_x
237 concentrations of Station B converged with that of Station A (0.31 ± 0.04 nM between 525–1201
238 m), even though sampled in different years. The Station A (2013) and Station B (2014) MnO_x
239 profiles diverged at 2000 m (Figs. 2 & 3); at Station A, MnO_x decreased to 0.19 nM whereas, at
240 Station B, MnO_x increased to 0.5 nM and continued increasing with depth to 3.5 nM MnO_x at
241 2600 m.

242 The average Mn(III)-L_{DFOB} at Station A was 0.14 nM (range: detection limit (0.008 nM)
243 to 0.31 nM) and at Station B it was 0.43 nM (range: 0.17 to 0.83 nM) (Table 1). Mn(III)-L_{DFOB}
244 profiles (Figs. 2 & 3) are atypical for a nutrient species initially sourced *via* atmospheric

245 deposition (Jickells et al., 2016). The expectation was that the Mn(III)-L_{DFOB} profiles would
246 follow that of manganese(II), high at the surface and concentrations decrease with depth as it
247 adsorbed onto sinking particles. Mn(III)-L_{DFOB} profiles, however, were more similar to nutrient
248 style profiles; these biologically controlled profiles exhibit low concentrations at the surface, a
249 subsurface maximum before concentrations decrease with depth. The Mn(III)-L_{DFOB} subsurface
250 maximum corresponded to the salinity maximum at all stations (Figs. 2 & 3). In contrast to many
251 trace nutrient species, Mn(III)-L_{DFOB} concentrations increased with depth (~ 0.07 nM per 1000
252 m); this increase was not linear as some variability occurred. Mn(III)-L_{DFOB} minima occurred in
253 sunlit surface water, at the oxygen minimum and during the transition from the OMZ to
254 intermediate waters. Mn(III)-L_{DFOB} maxima occurred at the base of the euphotic zone (~ 100 m),
255 below the oxygen minimum and at depth. From the lower OMZ boundary into the deeper water,
256 Mn(III)-L_{DFOB} concentrations increased by a factor of 2–3 with depth (Table 1, Figs. 2 & 3).

257 **4.0 Discussion**

258 The collection of samples for the measurement of particulate MnO_x, dissolved Mn(III)-
259 L_{DFOB}, and dMn_T took place during the profiling of four Stations in the Northwest Atlantic
260 Ocean in August 2013 and 2014 (Figs. 2–5). These profiles, pairs of stations intended as repeat
261 profiles, traversed the regional OMZ off the margin of the continental shelf. In surface waters
262 shallower than 45 m, the concentrations of dMn_T were similar to Shiller (1997) but lower (7 ± 1
263 *versus* 35 ± 24 nM) than observed by Oldham et al. (2020) in August 2017 in surface waters (<
264 54 m) at a shelf station (OLH04; Fig. 1). However, the Oldham et al. (2020) MnO_x
265 concentrations (1.1 ± 0.9 nM), which were measured using the LBB technique, were similar to
266 our concentrations (1.0 ± 0.8). In our surface water samples, manganese(II) was the dominant
267 species (Table 1 and Figs. 2 & 3) in agreement with Sunda et al. (1983). However, this

268 observation is at odds with organic-rich near-surface waters (< 3 m) of the Saguenay Fjord in
269 Canada (Jones et al., 2019a), and NW Atlantic shelf waters (Oldham et al., 2020) where
270 manganese(III) was dominant. Nevertheless, throughout the water column of the Northwest
271 Atlantic, manganese(II) was generally the dominant species (Table 2, Figs. 4 & 5).

272 The intermediate and deep water dMn_T concentrations are approximately 10-times higher
273 than the 2011 winter measured US GEOTRACES NW Atlantic US continental shelf-slope
274 station (USGT11-01) and 3–4 times higher than USGT11-06 (Fig. 1; Wu et al., 2014). Our dMn_T
275 samples show a similarity in their concentration and depth profile to samples collected ~ 420 km
276 off the Japanese shelf-slope in the North West Pacific Ocean (Morton et al., 2019). The dMn_T
277 range in those Pacific samples, influenced by lateral inputs of material, was 0.7–6.3 nM with the
278 maximum at 650 m (106 µM O_2) (Morton et al., 2019). However, as approximately 60% of shelf
279 inputs of dMn_T will be lost within < 1000 km, lateral inputs of dissolved manganese are unlikely
280 to be far-reaching with respect to oceanic basin scale (Middag et al., 2011; Noble et al., 2012).
281 Comparing our samples and GEOTRACES USGT11-06, the magnitude of dMn_T decrease
282 approximates the trend with distance from the shelf observed by Noble et al. (2012); our samples
283 were collected ~ 60 km off the slope and USGT11-06 ~ 500 km.

284 The measurement of MnO_x using the organic dye leucoberbelin blue occurs because of
285 the ability of MnO_x to oxidize organics, in this case through a hydrogen atom transfer (Jones et
286 al., 2019a; Luther et al., 2018). Although the LBB analytical method is conducted at ~ pH 4 to
287 ensure a rapid and complete reaction, LBB reactivity is indicative of the ability of MnO_x to
288 oxidize natural organic material. The LBB reaction thus mimics a fundamental step in a wide
289 range of environmental processes (Mayer, 2011). Weakly complexed manganese(III) (log K_{COND}
290 < 13.2 in seawater (Luther et al., 2015)) is also capable of oxidizing LBB through hydrogen atom

291 transfer and is present in marine and estuarine environments (Jones et al., 2019b). DFOB is a
292 strong ligand (log K_{COND} =13.2 in seawater (Luther et al., 2015)) that outcompetes weak ligands
293 stabilizing manganese(III) in complexes that oxidize LBB (Jones et al., 2019a). Therefore, the
294 DFOB technique provides a means of quantifying, at minimum, the LBB reactive pool of
295 manganese(III) (Jones et al., 2019a). The concentrations of MnO_x between 100 and 1000 m are
296 in good agreement (0.2–0.8 nM) with particulate manganese measurements from GEOTRACES
297 Stations USGT11-01 and USGT11-06 (Twining et al., 2015). The concentrations of Mn(III)-
298 L_{DFOB} are similar to those measured in North Atlantic seawater (S_p > 32) flowing into the Gulf of
299 St. Lawrence, Mn(III)-L_{DFOB}, 0.73–1.1 nM (Jones et al., 2019b). In comparison, our mean
300 Mn(III)-L_{DFOB} concentration at the A Stations was 0.14 nM and at the B Stations, 0.43 nM, the B
301 Stations maximum was 0.83 nM and at 34 m.

302 At our location, manganese in the water column comes from atmospheric deposition
303 (Baker et al., 2016, 2006), fluxes from rivers and out of sediments from across the shelf (Burdige
304 and Komada, 2020; Charette et al., 2016), and horizontal transport of plumes of dissolved and
305 particulate manganese sourced from the shelf-slope (for example, Martin et al. (1985) and
306 Morten et al. (2019) and references therein). This region has high surface water dMn_T, attributed
307 to both reductive dissolution of manganese particles in aerosols and advection from the shelf
308 (Shiller, 1997). Inputs of dust are seasonal and are higher in summer than winter (Adams et al.,
309 2012; Liu et al., 2008); similar observations have been reported for dissolved iron in surface
310 waters (Wu and Luther, 1996, 1994). The elevated dMn_T measured at Stations A and B relative
311 to GEOTRACES Stations may, therefore, be a combination of differences in seasonal
312 atmospheric deposition and lateral inputs from the shelf and continental slope as our stations are
313 close to the shelf.

4.1 Manganese redox cycling

Manganese(II) oxidation is most likely to occur as two single-electron transfers (Luther, 2010), of which there are two pathways. The primary pathway is through microbial catalysis (Clement et al., 2009; Emerson et al., 1982). The secondary pathway includes all abiotic reactions. Generally, oxidation of manganese(II) by molecular oxygen is slow (Morgan, 2005; von Langen et al., 1997) so other oxidants are required, for example, superoxide (Hansard et al., 2011), which is likely prevalent in marine systems (Sutherland et al., 2020). When sufficient concentrations of ligands are present, the first single-electron transfer results in a ligand stabilized manganese(III) (Klewicki and Morgan, 1998; Kostka et al., 1995; Pakhomova et al., 2009; Parker et al., 2004; Webb et al., 2005). If there are insufficient ligands, the oxidation of manganese(II) rapidly produces MnO_x (Butterfield et al., 2013; Soldatova et al., 2017a, 2017b).

Manganese(III/IV) oxide particles may oxidize ambient dissolved organic matter resulting in Mn(III)-L_{DFOB} and manganese(II) (Duckworth and Sposito, 2007, 2005b; Klewicki and Morgan, 1999). Mn(III)-L_{DFOB} is produced because the oxidized low molecular weight organic material (Sunda and Kieber, 1994) will form stable complexes with the concomitantly produced manganese(III) (Jones et al., 2019a; Klewicki and Morgan, 1998; Launer and Yost, 1934; Magliozzo and Marcinkeviciene, 1997). We found that MnO_x was present throughout the water column, albeit, generally at sub-nanomolar concentrations. This finding agrees with work that used sequential extraction of particulate material collected at depth in the North Atlantic, which showed that under normal atmospheric loading, MnO_2 accounts for 70% of oceanic particulate manganese (Lam et al., 2015).

4.2 Manganese speciation at the base of the euphotic zone

High concentrations of MnO_x and Mn(III)-L_{DFOB} occurred at the base of the euphotic zone (Table 1 and Figs. 2 & 3), a depth approximately corresponding to the deep chlorophyll maxima (DCM) (Cox et al., 1982; Cullen, 1982; Sunda and Huntsman, 1997). MnO_2 (MnO_x, 1.1 ± 0.4 nM) formation commonly occurs in the DCM (Sunda and Huntsman, 1988). At the DCM, sinking phytoplankton help to produce elevated nutrients (Huisman et al., 2006) and a relatively dense bacterial community, which respires organic material (containing oxidized manganese in photosystem-II), conditions also leading to manganese(III) formation/stabilization. Since the DCM is iron-limited (Hogle et al., 2018), the formation of Mn(III)-L will exacerbate iron limitation as manganese(III) provides direct competition with iron(III) for stabilization by siderophores (Luther et al., 2015). For example, manganese(III) binds to siderophore hydroxamate motifs (Parker et al., 2004) with a higher affinity than iron(III), and the concentration of manganese(III) (0.41 ± 0.09 nM) is approximately 20-fold higher than the hydroxamate siderophore concentration (up to 0.02 nM (Mawji et al., 2008)). With manganese(III) more abundant than iron(III), it will compete with iron(III) even if it has a lower affinity.

4.3 Manganese at mid-depth

In surface waters, inhibition of MnO_x formation and the near-complete removal of MnO_x occurs because of photochemical inhibition and reduction (Sunda et al., 1983; Sunda and Huntsman, 1994, 1988). Therefore, the initial formation of Mn(III)-L and MnO_x below the euphotic zone requires the oxidation of manganese(II). The mid-depth MnO_x layer (Station B, 448 m) and the nepheloid layer, with high manganese(II) and MnO_x, indicate insufficient ligands were present to prevent the oxidative pathway from completing to MnO_x. The similarity in manganese speciation relationships (high manganese(II) and MnO_x and low Mn(III)-L) to those of the benthic

359 nepheloid layer in the St. Lawrence Estuary (Oldham et al., 2017b) support the observations of
360 Morton et al. (2019) and Bishop and Fleisher (1987) that our dMn_T and MnO_x are transported
361 laterally from sedimentary sources on the shelf and slope. Either, MnO_x is directly sourced from
362 the sediment or, through biotic (Emerson et al., 1982; Tebo, 1991; Tebo et al., 2004) and abiotic
363 processes, is formed in situ during lateral transport either producing or accreting on small (1–4
364 μm) neutrally buoyant particles (Bishop and Fleisher, 1987; Lam et al., 2012; Sundby et al.,
365 1981). A diffuse MnO_x layer increases the availability for particle water interactions and
366 consequently, an increase in reaction rates per volume (Rutgers van der Loeff and Boudreau,
367 1997). If formed *in situ*, the MnO_x can sequester organic carbon (Estes et al., 2017; Johnson et
368 al., 2015) and trace nutrients (phosphorus and iron; Murray, 1975) from their surrounding water.

369 The oxidizing capacity of manganese species derives from the number of electrons each
370 accepts and their redox potential, which are determined by the relative strength of the Mn(III)-L
371 complexes in the soluble phase or the crystallinity, sorbed materials and nature of the solid
372 manganese(III,IV) species. Weak Mn(III)-L complexes are likely redox reactive and the ligand
373 relatively bioavailable (Beyer Jr. and Fridovich, 1989; Jones et al., 2019a; Klewicki and Morgan,
374 1998; Sunda and Kieber, 1994). If the ligands are organic acids, the manganese(III) can reduce
375 the carboxyl motifs to carbon dioxide (Klewicki and Morgan, 1999, 1998). The presence of
376 Mn(III)-L_{DFOB} increases the oxidizing capability of the soluble phase (Sun et al., 2015; Tian et
377 al., 2019), which has a longer residence time relative to the particulate phase. Manganese oxide
378 particles may also have a relatively long residence time as the rate they sink (~ 0.76 m d^{-1}) is low
379 relative to Stokes Law (Glockzin et al., 2014). Glockzin et al. (2014) attribute the slow MnO_x
380 sinking rate to the entrapment of MnO_x within an organic matrix, which suggests a bacterial
381 formation of MnO_x based on laboratory studies (Toner et al., 2005). Nevertheless, sedimentary

382 sourced particles may also play a role in extending the residence time and influencing lateral
383 transport of MnO_x. The MnO_x particles could be sourced directly from surficial (oxidized)
384 sediments or the benthic boundary layer and advected laterally, or they could be formed in situ
385 during transport of other particles. For example, small (1–4 μm) pyrite crystals are relatively
386 neutrally buoyant and undergo orders of magnitude greater lateral transport (100s km) than
387 vertical (10s m) transport (Lam et al., 2012). Over hundreds of kilometers of lateral transport in
388 ~ 100 d, up to 100% of 1 μm pyrite and 35% of 4 μm pyrite will oxidize (Lam et al., 2012). The
389 oxidation of continental margin sourced pyrite during lateral transport results in a diffuse high
390 concentration of small neutrally buoyant iron oxyhydroxide particles that provide a large surface,
391 which may act as a catalyst for MnO_x formation.

392 A prominent zone of oxidized manganese species at depth included 2–3 nM MnO_x at
393 Station B (448 m; Fig. 3) and a broad Mn(III)-L_{DFOB} maximum [0.31 nM at 402 m, Station A
394 (Fig. 2); 0.6 nM at 371 and 448 m, Station B (Fig. 3)]. Though the oxidized manganese layer was
395 within the same range as the OMZ, the OMZ in this region contains sufficient oxygen such that
396 alternate respiratory electron acceptors such as MnO_x are not likely to be used. At both stations,
397 elevated MnO_x was at the base of, or below, the Mn(III)-L_{DFOB} layer, and this location highlights
398 the current paradigm in manganese biogeochemistry. Either, following the oxidation of Mn(III)-
399 L_{DFOB}, the MnO_x settled through the water column, or during MnO_x lateral transport, which has a
400 low (< 1 m d^{-1}) vertical component (Glockzin et al., 2014; Lam et al., 2012), the Mn(III)-L_{DFOB}
401 layer formed due to the MnO_x reacting with sinking organic material. Diffuse reactive oxidized
402 manganese layers are highly efficient in capturing and breaking down organic carbon (Rutgers
403 van der Loeff and Boudreau, 1997) with similar processes that occur at the sediment water
404 interface (Hedges and Keil, 1995; Madison et al., 2013).

4.4 The nepheloid layer

The nepheloid layer at depth at Station B is an example of a significant continental slope input into the water column. The nepheloid layer(s) occurs as waters flush through the Wilmington and Baltimore submarine canyons (Canals et al., 2006; Puig et al., 2013). GEOTRACES observed Nepheloid layers containing > 15 nM MnO_2 at Stations USGT11-04, -06, -08, and -10 during their winter 2011 cruise (Fig. 1 and Lam et al., 2015); the nepheloid layer at Station USGT11-10 was 1100 m thick. At the shelf-slope, nepheloid layer(s) would likely combine high concentrations of manganese(II) from the oxygen-deficient interstitial pore waters and high concentrations of MnO_x from the sub-oxic interface. A manganese speciation profile similar to the bottom waters of Station B occurs in the benthic nepheloid layer of the outer St. Lawrence Estuary (Jones et al., 2019a; Oldham et al., 2017b). In contrast to our observations, the particulate manganese nepheloid layers observed in the GEOTRACES program (Lam et al., 2015) did not contain an enrichment of dMn_T (Wu et al., 2014). The difference in manganese fractions suggests removal of dMn_T since nepheloid layer formation.

4.5 Relevance of manganese(III)

Manganese(III) occurs in two pools of manganese, the oxidized and the dissolved pools. The oxidized pool includes manganese species known for their oxidizing capacity ($_{oxi}Mn$; Figs. 4 & 5). It is inclusive of both soluble and particulate phases, Mn(III)-L_{DFOB} and MnO_x ($_{oxi}Mn$ = Mn(III)-L_{DFOB} + MnO_x), respectively. The soluble manganese pool contains species capable of being oxidized, dMn_T (dMn_T = manganese(II) + Mn(III)-L_{DFOB}; Figs. 4 & 5). The dMn_T pool may contain other soluble oxidized species of manganese at low concentrations (< 0.3 nM; (Thibault de Chanvalon and Luther, 2019)), which may not react with DFOB under the

427 conditions used. Below the euphotic zone and between years, there is a difference in the relative
428 concentrations of manganese species. In 2013, $_{oxi}$Mn was equivalent to 25% of the total
429 manganese (Mn_T), whereas, in 2014, it was closer to 45% (Table 2 and Figs. 4 & 5). The
430 difference in the contribution indicates that significant changes can pervade the underlying redox
431 behavior of an oceanic water column (Figs. 4 & 5). One contributing factor may be the seasonal
432 phytoplankton bloom, which was greater at Station A than Station B (Fig. 6), and following its
433 collapse, the available organic carbon provided a mechanism to induce greater manganese
434 cycling resulting in different concentrations of Mn(III)-L_{DFOB}.

435 Though the concentration of Mn(III)-L_{DFOB} is spatially variable, there are three
436 underlying trends. First, Mn(III)-L_{DFOB} increases within the $_{oxi}$Mn pool with depth (Figs. 4 & 5),
437 from < 10% at the surface to up to 60% by 2000 m. Increasing Mn(III)-L_{DFOB} suggests that, even
438 with the aging of the mineral lattice (Eitel et al., 2018) during MnO_x horizontal and vertical
439 transport, MnO_x retain some capacity to oxidize available organic material. The second and third
440 trends are, Mn(III)-L_{DFOB} increasing in concentration with depth (Table 1, Figs. 2 & 3) and
441 increasing proportionally within dMn_T with depth, from 1 to 23% (Table 2, Figs. 4 & 5). These
442 trends may help explain why dMn_T concentrations in intermediate and deep oceanic waters are
443 higher than predicted from the modeling of an ion removed through scavenging onto suspended
444 particulate material (Martin and Knauer, 1984; Statham et al., 1998; Sunda and Huntsman,
445 1988). To account for the higher than expected residence time and concentration of dMn_T, redox
446 cycling of manganese in marine systems (Sunda and Huntsman, 1988) must replenish the dMn_T
447 from MnO_x. Therefore, MnO_x particles play an essential role in elemental cycles in the ocean.
448 This cycling supports the theory that deep oceanic water dMn_T contains significant quantities of
449 Mn(III)-L (Johnson, 2006) within the global ocean's uniform dissolved manganese concentration

of 0.15 nM (Statham et al., 1998).

5.0 Conclusion

Through direct quantification of 1) reactive MnO_x (Jones et al., 2019a), as opposed to estimating MnO_2 from sequential leaching of particulate manganese, and 2) measuring reactive Mn(III)-L (Jones et al., 2019a, 2019b), we have quantified the oxidized intermediate- and end-member in the manganese cycle. MnO_x and Mn(III)-L are redox reactive, participating in electron transfer and hydrogen atom transfer reactions (Jones et al., 2019a; Luther et al., 2018), and are intrinsically linked to organic carbon. In oxygenated systems, these oxidized species dominate manganese cycling. Mn(III)-L is pervasive in marine systems, and this characteristic means it is a significant component of the deep water-soluble manganese. Mn(III)-L will also play a role as a reductant or oxidant in this system. In the oceanic water column, the dynamic nature of MnO_x and likely Mn(III)-L suggest that the cycling of these species will significantly affect marine biogeochemistry and especially that of organic carbon.

Acknowledgments

This work was supported primarily by research grants from the Chemical Oceanography Program of the National Science Foundation (OCE-1558692 and OCE-1154357 to BMT and OCE-1558738 and OCE-1155385 to GWL) with partial support from the U.S. National Oceanic and Atmospheric Administration Sea Grant program (NA14OAR4170087 to GWL). We are also grateful to the captains and crew of the R/V *Hugh R Sharp* who made the sampling for this research possible and highly hospitable. In addition, we thank the reviewers for their excellent comments and suggestions that helped with improving this paper.

Bibliography

Adams, A.M., Prospero, J.M., Zhang, C., 2012. CALIPSO-derived three-dimensional structure of aerosol over the Atlantic basin and adjacent continents. J. Clim. 25, 6862–6879. https://doi.org/10.1175/JCLI-D-11-00672.1

Aguilar-Islas, A.M., Resing, J.A., Bruland, K.W., 2006. Catalytically enhanced spectrophotometric determination of manganese in seawater by flow-injection analysis with a commercially available resin for on-line preconcentration. Limnol. Oceanogr. Methods 4, 105–113. https://doi.org/10.4319/lom.2006.4.105

Altmann, H.J., 1972. Bestimmung von in wasser gelostem sauerstoff mit Leukoberbelinblau I. Eine schnelle Winkler-Methode. Z Anal Chem 262, 97–99. http://aquaticcommons.org/4843/1/68_1972_altm_dete.pdf

Baker, A.R., Jickells, T.D., Witt, M., Linge, K.L., 2006. Trends in the solubility of iron, aluminium, manganese and phosphorus in aerosol collected over the Atlantic Ocean. Mar. Chem. 98, 43–58.

Baker, A.R., Landing, W.M., Bucciarelli, E., Cheize, M., Fietz, S., Hayes, C.T., Kadko, D., Morton, P.L., Rogan, N., Sarthou, G., Shelley, R.U., Shi, Z., Shiller, A., van Hulten, M.M.P., 2016. Trace element and isotope deposition across the air–sea interface: progress and research needs. Philos. Trans. R. Soc. Math. Phys. Eng. Sci. 374, 20160190. https://doi.org/10.1098/rsta.2016.0190

Beyer Jr., W.F., Fridovich, I., 1989. Characterization of a superoxide dismutase mimic prepared from desferrioxamine and MnO_2. Arch. Biochem. Biophys. 271, 149–156. https://doi.org/10.1016/0003-9861(89)90265-8

Bishop, J.K.B., Fleisher, M.Q., 1987. Particulate manganese dynamics in Gulf Stream warm-core rings and surrounding waters of the N.W. Atlantic. Geochim. Cosmochim. Acta 51, 2807–2825. https://doi.org/10.1016/0016-7037(87)90160-8

Boyd, P.W., Claustre, H., Levy, M., Siegel, D.A., Weber, T., 2019. Multi-faceted particle pumps drive carbon sequestration in the ocean. Nature 568, 327. https://doi.org/10.1038/s41586-019-1098-2

Burdige, D.J., Komada, T., 2020. Iron redox cycling, sediment resuspension and the role of sediments in low oxygen environments as sources of iron to the water column. Mar. Chem. 223, 103793. https://doi.org/10.1016/j.marchem.2020.103793

Butterfield, C.N., Soldatova, A.V., Lee, S.-W., Spiro, T.G., Tebo, B.M., 2013. Mn(II,III) oxidation and MnO_2 mineralization by an expressed bacterial multicopper oxidase. Proc. Natl. Acad. Sci. 110, 11731–11735. https://doi.org/10.1073/pnas.1303677110

Canals, M., Puig, P., Madron, X.D. de, Heussner, S., Palanques, A., Fabres, J., 2006. Flushing submarine canyons. Nature 444, 354–357. https://doi.org/10.1038/nature05271

Chang Chien, S.W., Chen, H.L., Wang, M.C., Seshaiah, K., 2009. Oxidative degradation and associated mineralization of catechol, hydroquinone and resorcinol catalyzed by birnessite. Chemosphere 74, 1125–1133. https://doi.org/10.1016/j.chemosphere.2008.10.007

Charette, M.A., Lam, P.J., Lohan, M.C., Kwon, E.Y., Hatje, V., Jeandel, C., Shiller, A.M., Cutter, G.A., Thomas, A., Boyd, P.W., Homoky, W.B., Milne, A., Thomas, H., Andersson, P.S., Porcelli, D., Tanaka, T., Geibert, W., Dehairs, F., Garcia-Orellana, J., 2016. Coastal ocean and shelf-sea biogeochemical cycling of trace elements and isotopes: lessons learned from GEOTRACES. Philos. Trans. R. Soc. Math. Phys. Eng. Sci. 374, 20160076. https://doi.org/10.1098/rsta.2016.0076

Chorover, J., Amistadi, M.K., 2001. Reaction of forest floor organic matter at goethite, birnessite and smectite surfaces. Geochim. Cosmochim. Acta 65, 95–109. https://doi.org/10.1016/S0016-7037(00)00511-1

Clement, B.G., Luther, G.W., Tebo, B.M., 2009. Rapid, oxygen-dependent microbial Mn(II) oxidation kinetics at sub-micromolar oxygen concentrations in the Black Sea suboxic zone. Geochim. Cosmochim. Acta 73, 1878–1889. https://doi.org/10.1016/j.gca.2008.12.023

Cox, J.L., Wiebe, P.H., Ortner, P., Boyd, S., 1982. Seasonal development of subsurface chlorophyll maxima in slope water and northern Sargasso Sea of the Northwestern Atlantic Ocean. Biol. Oceanogr. 1, 271–285. https://doi.org/10.1080/01965581.1982.10749444

Cullen, J.J., 1982. The deep chlorophyll maximum: Comparing vertical profiles of chlorophyll a. Can. J. Fish. Aquat. Sci. 39, 791–803. https://doi.org/10.1139/f82-108

Davies, G., 1969. Some aspects of the chemistry of manganese(III) in aqueous solution. Coord. Chem. Rev. 4, 199–224. https://doi.org/10.1016/S0010-8545(00)80086-7

Dellwig, O., Schnetger, B., Brumsack, H.-J., Grossart, H.-P., Umlauf, L., 2012. Dissolved reactive manganese at pelagic redoxclines (part II): Hydrodynamic conditions for accumulation. J. Mar. Syst. 90, 31–41. https://doi.org/10.1016/j.jmarsys.2011.08.007

Duckworth, O.W., Sposito, G., 2007. Siderophore-promoted dissolution of synthetic and biogenic layer-type Mn oxides. Chem. Geol. 242, 497–508. https://doi.org/10.1016/j.chemgeo.2007.05.007

Duckworth, O.W., Sposito, G., 2005a. Siderophore−manganese(III) interactions. I. Air-oxidation of manganese(II) promoted by desferrioxamine B. Environ. Sci. Technol. 39, 6037–6044. https://doi.org/10.1021/es050275k

Duckworth, O.W., Sposito, G., 2005b. Siderophore−manganese(III) interactions II. Manganite dissolution promoted by desferrioxamine B. Environ. Sci. Technol. 39, 6045–6051. https://doi.org/10.1021/es050276c

Eitel, E.M., Zhao, S., Tang, Y., Taillefert, M., 2018. Effect of manganese oxide aging and structure transformation on the kinetics of thiol oxidation. Environ. Sci. Technol. 52, 13202–13211. https://doi.org/10.1021/acs.est.8b03993

Emerson, S., Kalhorn, S., Jacobs, L., Tebo, B.M., Nealson, K.H., Rosson, R.A., 1982. Environmental oxidation rate of manganese(II) - bacterial catalysis. Geochim. Cosmochim. Acta 46, 1073–1079.

Estes, E.R., Andeer, P.F., Nordlund, D., Wankel, S.D., Hansel, C.M., 2017. Biogenic manganese oxides as reservoirs of organic carbon and proteins in terrestrial and marine environments. Geobiology 15, 158–172. https://doi.org/10.1111/gbi.12195

Evans, R.H., Baker, K.S., Brown, O.B., Smith, R.C., 1985. Chronology of warm-core ring 82B. J. Geophys. Res. Oceans 90, 8803–8811. https://doi.org/10.1029/JC090iC05p08803

Glockzin, M., Pollehne, F., Dellwig, O., 2014. Stationary sinking velocity of authigenic manganese oxides at pelagic redoxclines. Mar. Chem. 160, 67–74. https://doi.org/10.1016/j.marchem.2014.01.008

Hansard, S.P., Easter, H.D., Voelker, B.M., 2011. Rapid reaction of nanomolar Mn(II) with superoxide radical in seawater and simulated freshwater. Environ. Sci. Technol. 45, 2811–2817.

562 Hedges, J.I., Keil, R.G., 1995. Sedimentary organic matter preservation: An assessment and
563 speculative synthesis. Mar. Chem. 49, 81–115. https://doi.org/10.1016/0304-
564 4203(95)00008-F
565 Hogle, S.L., Dupont, C.L., Hopkinson, B.M., King, A.L., Buck, K.N., Roe, K.L., Stuart, R.K.,
566 Allen, A.E., Mann, E.L., Johnson, Z.I., Barbeau, K.A., 2018. Pervasive iron limitation at
567 subsurface chlorophyll maxima of the California Current. Proc. Natl. Acad. Sci. 115,
568 13300–13305. https://doi.org/10.1073/pnas.1813192115
569 Huisman, J., Pham Thi, N.N., Karl, D.M., Sommeijer, B., 2006. Reduced mixing generates
570 oscillations and chaos in the oceanic deep chlorophyll maximum. Nature 439, 322–325.
571 https://doi.org/10.1038/nature04245
572 Jensen, L.T., Wyatt, N.J., Landing, W.M., Fitzsimmons, J.N., 2020. Assessment of the stability,
573 sorption, and exchangeability of marine dissolved and colloidal metals. Mar. Chem. 220,
574 103754. https://doi.org/10.1016/j.marchem.2020.103754
575 Jickells, T.D., Baker, A.R., Chance, R., 2016. Atmospheric transport of trace elements and
576 nutrients to the oceans. Philos. Trans. R. Soc. Math. Phys. Eng. Sci. 374, 20150286.
577 https://doi.org/10.1098/rsta.2015.0286
578 Johnson, K., Purvis, G., Lopez-Capel, E., Peacock, C., Gray, N., Wagner, T., März, C., Bowen,
579 L., Ojeda, J., Finlay, N., Robertson, S., Worrall, F., Greenwell, C., 2015. Towards a
580 mechanistic understanding of carbon stabilization in manganese oxides. Nat. Commun. 6,
581 7628. https://doi.org/10.1038/ncomms8628
582 Johnson, K.S., 2006. Manganese redox chemistry revisited. Science 313, 1896–1897.
583 https://doi.org/10.1126/science.1133496
584 Jones, M.R., Luther, G.W., Mucci, A., Tebo, B.M., 2019a. Concentrations of reactive Mn(III)-L
585 and MnO_2 in estuarine and marine waters determined using spectrophotometry and the
586 leuco base, leucoberbelin blue. Talanta 200, 91–99.
587 https://doi.org/10.1016/j.talanta.2019.03.026
588 Jones, M.R., Oldham, V.E., Luther, G.W., Mucci, A., Tebo, B.M., 2019b. Distribution of
589 desferrioxamine-B-extractable soluble manganese(III) and particulate MnO_2 in the St.
590 Lawrence Estuary, Canada. Mar. Chem. 208, 70–82.
591 https://doi.org/10.1016/j.marchem.2018.11.005
592 Joyce, T.M., Schmitt, R.W., Stalcup, M.C., 1983. Influence of the Gulf Stream upon the short-
593 term evolution of a warm-core ring. Mar. Freshw. Res. 34, 515–524.
594 https://doi.org/10.1071/mf9830515
595 Klewicki, J.K., Morgan, J.J., 1999. Dissolution of β-MnOOH particles by ligands:
596 pyrophosphate, ethylenediaminetetraacetate, and citrate. Geochim. Cosmochim. Acta 63,
597 3017–3024. https://doi.org/10.1016/S0016-7037(99)00229-X
598 Klewicki, J.K., Morgan, J.J., 1998. Kinetic behavior of Mn(III) complexes of pyrophosphate,
599 EDTA, and citrate. Environ. Sci. Technol. 32, 2916–2922.
600 https://doi.org/10.1021/es980308e
601 Kostka, J.E., Luther, G.W., Nealson, K.H., 1995. Chemical and biological reduction of Mn(III)-
602 pyrophosphate complexes: Potential importance of dissolved Mn(III) as an environmental
603 oxidant. Geochim. Cosmochim. Acta 59, 885–894.
604 Lam, P.J., Ohnemus, D.C., Auro, M.E., 2015. Size-fractionated major particle composition and
605 concentrations from the US GEOTRACES North Atlantic Zonal Transect. Deep Sea Res.
606 Part II Top. Stud. Oceanogr., GEOTRACES GA-03 - The U.S. GEOTRACES North
607 Atlantic Transect 116, 303–320. https://doi.org/10.1016/j.dsr2.2014.11.020

608 Lam, P.J., Ohnemus, D.C., Marcus, M.A., 2012. The speciation of marine particulate iron
609 adjacent to active and passive continental margins. Geochim. Cosmochim. Acta 80, 108–
610 124. https://doi.org/10.1016/j.gca.2011.11.044
611 Launer, H.F., Yost, D.M., 1934. The kinetics of the reaction between potassium permanganate
612 and oxalic acid. II. J. Am. Chem. Soc. 56, 2571–2577.
613 https://doi.org/10.1021/ja01327a013
614 Liu, D., Wang, Z., Liu, Z., Winker, D., Trepte, C., 2008. A height resolved global view of dust
615 aerosols from the first year CALIPSO lidar measurements. J. Geophys. Res. Atmospheres
616 113. https://doi.org/10.1029/2007JD009776
617 Luther, G.W., 2010. The role of one- and two-electron transfer reactions in forming
618 thermodynamically unstable intermediates as barriers in multi-electron redox reactions.
619 Aquat. Geochem. 16, 395–420. https://doi.org/10.1007/s10498-009-9082-3
620 Luther, G.W., 1990. The frontier-molecular-orbital theory approach in geochemical processes,
621 in: Stumm, W. (Ed.), Aquatic Chemical Kinetics. John Wiley & Sons Ltd, New York, pp.
622 173–198.
623 Luther, G.W., Chanvalon, A.T. de, Oldham, V.E., Estes, E.R., Tebo, B.M., Madison, A.S., 2018.
624 Reduction of manganese oxides: Thermodynamic, kinetic and mechanistic considerations
625 for one- versus two-electron transfer steps. Aquat. Geochem. 257–277.
626 https://doi.org/10.1007/s10498-018-9342-1
627 Luther, G.W., Madison, A.S., Mucci, A., Sundby, B., Oldham, V.E., 2015. A kinetic approach to
628 assess the strengths of ligands bound to soluble Mn(III). Mar. Chem., SCOR WG 139:
629 Organic Ligands – A Key Control on Trace Metal Biogeochemistry in the Ocean 173,
630 93–99. https://doi.org/10.1016/j.marchem.2014.09.006
631 Madison, A.S., Tebo, B.M., Mucci, A., Sundby, B., Luther, G.W., 2013. Abundant porewater
632 Mn(III) is a major component of the sedimentary redox system. Science 341, 875–878.
633 https://doi.org/10.1126/science.1241396
634 Magliozzo, R.S., Marcinkeviciene, J.A., 1997. The role of Mn(II)-peroxidase activity of
635 mycobacterial catalase-peroxidase in activation of the antibiotic isoniazid. J. Biol. Chem.
636 272, 8867–8870. https://doi.org/10.1074/jbc.272.14.8867
637 Martin, J.H., Knauer, G.A., 1984. VERTEX: manganese transport through oxygen minima. Earth
638 Planet. Sci. Lett. 67, 35–47. https://doi.org/10.1016/0012-821X(84)90036-0
639 Martin, J.H., Knauer, G.A., Broenkow, W.W., 1985. VERTEX: the lateral transport of
640 manganese in the northeast Pacific. Deep Sea Res. Part Oceanogr. Res. Pap. 32, 1405–
641 1427. https://doi.org/10.1016/0198-0149(85)90056-1
642 Mawji, E., Gledhill, M., Milton, J.A., Tarran, G.A., Ussher, S., Thompson, A., Wolff, G.A.,
643 Worsfold, P.J., Achterberg, E.P., 2008. Hydroxamate siderophores: Occurrence and
644 importance in the Atlantic Ocean. Environ. Sci. Technol. 42, 8675–8680.
645 https://doi.org/10.1021/es801884r
646 Mayer, J.M., 2011. Understanding hydrogen atom transfer: From bond strengths to Marcus
647 Theory. Acc. Chem. Res. 44, 36–46. https://doi.org/10.1021/ar100093z
648 Middag, R., de Baar, H.J.W., Laan, P., Klunder, M.B., 2011. Fluvial and hydrothermal input of
649 manganese into the Arctic Ocean. Geochim. Cosmochim. Acta 75, 2393–2408.
650 https://doi.org/10.1016/j.gca.2011.02.011
651 Milne, A., Landing, W., Bizimis, M., Morton, P., 2010. Determination of Mn, Fe, Co, Ni, Cu,
652 Zn, Cd and Pb in seawater using high resolution magnetic sector inductively coupled

mass spectrometry (HR-ICP-MS). Anal. Chim. Acta 665, 200–207. https://doi.org/10.1016/j.aca.2010.03.027

Morgan, J.J., 2005. Kinetics of reaction between O_2 and Mn(II) species in aqueous solutions. Geochim. Cosmochim. Acta 69, 35–48. https://doi.org/10.1016/j.gca.2004.06.013

Morton, P.L., Landing, W.M., Shiller, A.M., Moody, A., Kelly, T.D., Bizimis, M., Donat, J.R., De Carlo, E.H., Shacat, J., 2019. Shelf Inputs and Lateral Transport of Mn, Co, and Ce in the Western North Pacific Ocean. Front. Mar. Sci. 6. https://doi.org/10.3389/fmars.2019.00591

Murray, J.W., 1975. The interaction of metal ions at the manganese dioxide-solution interface. Geochim. Cosmochim. Acta 39, 505–519. https://doi.org/10.1016/0016-7037(75)90103-9

Noble, A.E., Lamborg, C.H., Ohnemus, D.C., Lam, P.J., Goepfert, T.J., Measures, C.I., Frame, C.H., Casciotti, K.L., DiTullio, G.R., Jennings, J., Saito, M.A., 2012. Basin-scale inputs of cobalt, iron, and manganese from the Benguela-Angola front to the South Atlantic Ocean. Limnol. Oceanogr. 57, 989–1010. https://doi.org/10.4319/lo.2012.57.4.0989

Oldham, V.E., Jones, M.R., Tebo, B.M., Luther, G.W., 2017a. Oxidative and reductive processes contributing to manganese cycling at oxic-anoxic interfaces. Mar. Chem., SI: Honoring Frank Millero 195, 122–128. https://doi.org/10.1016/j.marchem.2017.06.002

Oldham, V.E., Lamborg, C.H., Hansel, C.M., 2020. The spatial and temporal variability of Mn speciation in the coastal Northwest Atlantic Ocean. J. Geophys. Res. Oceans 125, e2019JC015167. https://doi.org/10.1029/2019JC015167

Oldham, V.E., Mucci, A., Tebo, B.M., Luther, G.W., 2017b. Soluble Mn(III)–L complexes are abundant in oxygenated waters and stabilized by humic ligands. Geochim. Cosmochim. Acta 199, 238–246. https://doi.org/10.1016/j.gca.2016.11.043

Oldham, V.E., Owings, S.M., Jones, M.R., Tebo, B.M., Luther, G.W., 2015. Evidence for the presence of strong Mn(III)-binding ligands in the water column of the Chesapeake Bay. Mar. Chem. 171, 58–66. https://doi.org/10.1016/j.marchem.2015.02.008

Oldham, V.E., Siebecker, M.G., Jones, M.R., Mucci, A., Tebo, B.M., Luther, G.W., 2019. The speciation and mobility of Mn and Fe in estuarine sediments. Aquat. Geochem. https://doi.org/10.1007/s10498-019-09351-0

Pakhomova, S.V., Rozanov, A.G., Yakushev, E.V., 2009. Dissolved and particulate forms of iron and manganese in the redox zone of the Black Sea. Oceanology 49, 773–787. https://doi.org/10.1134/S0001437009060046

Parker, D.L., Sposito, G., Tebo, B.M., 2004. Manganese(III) binding to a pyoverdine siderophore produced by a manganese(II)-oxidizing bacterium. Geochim. Cosmochim. Acta 68, 4809–4820. https://doi.org/10.1016/j.gca.2004.05.038

Puig, P., Madron, X.D. de, Salat, J., Schroeder, K., Martín, J., Karageorgis, A.P., Palanques, A., Roullier, F., Lopez-Jurado, J.L., Emelianov, M., Moutin, T., Houpert, L., 2013. Thick bottom nepheloid layers in the western Mediterranean generated by deep dense shelf water cascading. Prog. Oceanogr. 111, 1–23. https://doi.org/10.1016/j.pocean.2012.10.003

Rutgers van der Loeff, M.M., Boudreau, B.P., 1997. The effect of resuspension on chemical exchanges at the sediment-water interface in the deep sea — A modelling and natural radiotracer approach. J. Mar. Syst. 11, 305–342. https://doi.org/10.1016/S0924-7963(96)00128-5

Scharff, J.P., Genin, R., 1975. Chélates du manganese(II) avec des coordinats phénoliques: Partie I. Complexes simples binaires. Anal. Chim. Acta 78, 201–209. https://doi.org/10.1016/S0003-2670(01)84766-8

Schnetger, B., Dellwig, O., 2012. Dissolved reactive manganese at pelagic redoxclines (part I): A method for determination based on field experiments. J. Mar. Syst. 90, 23–30. https://doi.org/10.1016/j.jmarsys.2011.08.006

Shiller, A.M., 1997. Manganese in surface waters of the Atlantic Ocean. Geophys. Res. Lett. 24, 1495–1498. https://doi.org/10.1029/97GL01456

Soldatova, A.V., Romano, C.A., Tao, L., Stich, T.A., Casey, W.H., Britt, R.D., Tebo, B.M., Spiro, T.G., 2017a. Mn(II) oxidation by the multicopper oxidase complex Mnx: A coordinated two-stage Mn(II)/(III) and Mn(III)/(IV) mechanism. J. Am. Chem. Soc. 139, 11381–11391. https://doi.org/10.1021/jacs.7b02772

Soldatova, A.V., Tao, L., Romano, C.A., Stich, T.A., Casey, W.H., Britt, R.D., Tebo, B.M., Spiro, T.G., 2017b. Mn(II) oxidation by the multicopper oxidase complex Mnx: A binuclear activation mechanism. J. Am. Chem. Soc. 139, 11369–11380. https://doi.org/10.1021/jacs.7b02771

Søndergaard, M., Middelboe, M., 1995. A cross-system analysis of labile dissolved organic carbon. Mar. Ecol. Prog. Ser. 118, 283–294.

Statham, P.J., Yeats, P.A., Landing, W.M., 1998. Manganese in the eastern Atlantic Ocean: processes influencing deep and surface water distributions. Mar. Chem. 61, 55–68. https://doi.org/10.1016/S0304-4203(98)00007-3

Stumm, W., Morgan, J.J., 1996. Aquatic Chemistry - Chemical Equilibria and Rates in Natural Waters. John Wiley and Son, New York.

Sun, B., Guan, X., Fang, J., Tratnyek, P.G., 2015. Activation of manganese oxidants with bisulfite for enhanced oxidation of organic contaminants: The involvement of Mn(III). Environ. Sci. Technol. 49, 12414–12421. https://doi.org/10.1021/acs.est.5b03111

Sunda, W.G., Huntsman, S.A., 1997. Interrelated influence of iron, light and cell size on marine phytoplankton growth. Nature 390, 389–392. https://doi.org/10.1038/37093

Sunda, W.G., Huntsman, S.A., 1994. Photoreduction of manganese oxides in seawater. Mar. Chem. 46, 133–152.

Sunda, W.G., Huntsman, S.A., 1988. Effect of sunlight on redox cycles of manganese in the southwestern Sargasso Sea. Deep-Sea Res. Part -Oceanogr. Res. Pap. 35, 1297–1317.

Sunda, W.G., Huntsman, S.A., Harvey, G.R., 1983. Photo-reduction of manganese oxides in seawater and its geochemical and biological implications. Nature 301, 234–236.

Sunda, W.G., Kieber, D.J., 1994. Oxidation of humic substances by manganese oxides yields low-molecular-weight organic substrates. Nature 367, 62–64. https://doi.org/10.1038/367062a0

Sundby, B., Silverberg, N., Chesselet, R., 1981. Pathways of manganese in an open estuarine system. Geochim. Cosmochim. Acta 45, 293–307. https://doi.org/10.1016/0016-7037(81)90240-4

Sutherland, K.M., Wankel, S.D., Hansel, C.M., 2020. Dark biological superoxide production as a significant flux and sink of marine dissolved oxygen. Proc. Natl. Acad. Sci. https://doi.org/10.1073/pnas.1912313117

Tebo, B.M., 1991. Manganese(II) oxidation in the suboxic zone of the Black Sea. Deep Sea Res. Part Oceanogr. Res. Pap., Black Sea Oceanography: Results from the 1988 Black Sea Expedition 38, S883–S905. https://doi.org/10.1016/S0198-0149(10)80015-9

743 Tebo, B.M., Bargar, J.R., Clement, B.G., Dick, G.J., Murray, K.J., Parker, D., Verity, R., Webb,
744 S.M., 2004. Biogenic manganese oxides: Properties and mechanisms of formation. Annu.
745 Rev. Earth Planet. Sci. 32, 287–328.
746 https://doi.org/10.1146/annurev.earth.32.101802.120213
747 Thibault de Chanvalon, A., Luther, G.W., 2019. Mn speciation at nanomolar concentrations with
748 a porphyrin competitive ligand and UV–vis measurements. Talanta 200, 15–21.
749 https://doi.org/10.1016/j.talanta.2019.02.069
750 Tian, S.-Q., Wang, L., Liu, Y.-L., Yang, T., Huang, Z.-S., Wang, X.-S., He, H.-Y., Jiang, J., Ma,
751 J., 2019. Enhanced permanganate oxidation of sulfamethoxazole and removal of
752 dissolved organics with biochar: Formation of highly oxidative manganese intermediate
753 species and in situ activation of biochar. Environ. Sci. Technol.
754 https://doi.org/10.1021/acs.est.9b00180
755 Toner, B., Fakra, S., Villalobos, M., Warwick, T., Sposito, G., 2005. Spatially resolved
756 characterization of biogenic manganese oxide production within a bacterial biofilm.
757 Appl. Environ. Microbiol. 71, 1300–1310. https://doi.org/10.1128/AEM.71.3.1300-
758 1310.2005
759 Trouwborst, R.E., Clement, B.G., Tebo, B.M., Glazer, B.T., Luther, G.W., 2006. Soluble Mn(III)
760 in suboxic zones. Science 313, 1955–1957.
761 Twining, B.S., Rauschenberg, S., Morton, P.L., Ohnemus, D.C., Lam, P.J., 2015. Comparison of
762 particulate trace element concentrations in the North Atlantic Ocean as determined with
763 discrete bottle sampling and in situ pumping. Deep Sea Res. Part II Top. Stud. Oceanogr.,
764 GEOTRACES GA-03 - The U.S. GEOTRACES North Atlantic Transect 116, 273–282.
765 https://doi.org/10.1016/j.dsr2.2014.11.005
766 von Langen, P.J., Johnson, K.S., Coale, K.H., Elrod, V.A., 1997. Oxidation kinetics of
767 manganese (II) in seawater at nanomolar concentrations. Geochim. Cosmochim. Acta 61,
768 4945–4954. https://doi.org/10.1016/S0016-7037(97)00355-4
769 Webb, S.M., Dick, G.J., Bargar, J.R., Tebo, B.M., 2005. Evidence for the presence of Mn(III)
770 intermediates in the bacterial oxidation of Mn(II). Proc. Natl. Acad. Sci. U. S. A. 102,
771 5558–5563. https://doi.org/10.1073/pnas.0409119102
772 Wu, J., Luther, G.W., 1996. Spatial and temporal distribution of iron in the surface water of the
773 northwestern Atlantic Ocean. Geochim. Cosmochim. Acta 60, 2729–2741.
774 https://doi.org/10.1016/0016-7037(96)00135-4
775 Wu, J., Luther, G.W., 1994. Size-fractionated iron concentrations in the water column of the
776 western North Atlantic Ocean. Limnol. Oceanogr. 39, 1119–1129.
777 https://doi.org/10.4319/lo.1994.39.5.1119
778 Wu, J., Roshan, S., Chen, G., 2014. The distribution of dissolved manganese in the tropical–
779 subtropical North Atlantic during US GEOTRACES 2010 and 2011 cruises. Mar. Chem.
780 166, 9–24. https://doi.org/10.1016/j.marchem.2014.08.007
781 Yao, W., Millero, F.J., 1996. Adsorption of phosphate on manganese dioxide in seawater.
782 Environ. Sci. Technol. 30, 536–541. https://doi.org/10.1021/es950290x
783

784 Table 1. The physicochemical values, oxygen concentration and percentage saturation (O_2 sat.), and manganese species concentration
785 for A (2013) and B (2014) Stations. The manganese species are particulate manganese(III/IV) oxide (MnO_x), total dissolved
786 manganese (dMn_T), soluble Mn(III)-L_{DFOB}, and the estimated manganese(II) (dMn_T - Mn(III)-L_{DFOB}). MnO_x errors are the standard
787 deviation of repeat analyses plus the error due to the regression of the calibration curve; dMn_T and Mn(III)-L_{DFOB} errors are the
788 standard deviation of triplicate analyses. The manganese(II) error was calculated through error propagation.

Depth	Temperature	Salinity	O_2	O_2 sat.	MnO_x	dMn_T	Mn(III)-L_{DFOB}	manganese(II)
m	°C	S_p	µM	%	nM	nM	nM	nM
Station A1 (37 07.84 N, 073 19.72 W; St. #7)								
10	27.7	35.74	192	95	0.49 ± 0.02	12.34 ± 0.04	0.02 ± 0.01	12.32 ± 0.04
74	16.8	35.87	244	64	1.22 ± 0.04	4.31 ± 0.08	0.31 ± 0.01	4.00 ± 0.08
154	14.0	35.81	258	56	0.89 ± 0.03	7.95 ± 0.03	0.23 ± 0.01	7.72 ± 0.03
225	11.9	35.48	126	47	0.49 ± 0.01	1.48 ± 0.04	0.09 ± 0.00	1.39 ± 0.04
402	7.1	35.09	171	57	0.40 ± 0.01	2.69 ± 0.03	0.31 ± 0.01	2.39 ± 0.03
698	5.0	35.01	231	73	0.27 ± 0.01	1.95 ± 0.05	0.13 ± 0.01	1.82 ± 0.05
Station A2 (37 18.45 N, 073 23.79 W; St. #12)								
5	27.6	35.73	191	95	0.81 ± 0.03	9.27 ± 0.05	0.07 ± 0.00	9.21 ± 0.05
152	13.5	35.73	212	81	1.30 ± 0.04	4.55 ± 0.02	0.21 ± 0.01	4.34 ± 0.02
256	12.6	35.63	177	67	0.92 ± 0.03	5.12 ± 0.12	0.00 ± 0.01	5.12 ± 0.12
325	10.2	35.29	130	46	0.29 ± 0.01	3.19 ± 0.19	0.02 ± 0.01	3.17 ± 0.19
525	6.2	35.05	194	63	0.26 ± 0.01	2.70 ± 0.19	0.13 ± 0.01	2.56 ± 0.19
825	4.7	34.99	240	75	0.34 ± 0.01	2.01 ± 0.00	0.10 ± 0.01	1.91 ± 0.01
Station A2 deep water (37 18.32 N, 073 24.03 W; St. #12A)								
2032	3.4	34.94	255	77	0.19 ± 0.01	1.38 ± 0.18	0.18 ± 0.01	1.20 ± 0.18
Station B1 (38 17.40 N, 072 43.70 W; St. #9)								
11	24.2	35.23	205	96	0.88 ± 0.07	6.43 ± 0.32	0.19 ± 0.03	6.24 ± 0.32
44	18.7	35.35	233	99	0.79 ± 0.08	6.10 ± 0.49	0.35 ± 0.08	5.75 ± 0.50
63	16.2	35.57	191	77	0.70 ± 0.03	2.86 ± 0.20	0.39 ± 0.01	2.47 ± 0.20
98	14.5	35.71	168	66	0.73 ± 0.04	2.28 ± 0.13	0.46 ± 0.02	1.82 ± 0.14
194	12.3	35.55	150	56	0.70 ± 0.02	1.48 ± 0.12	0.19 ± 0.05	1.29 ± 0.13
282	9.9	35.26	131	47	0.52 ± 0.03	1.31 ± 0.11	0.17 ± 0.07	1.14 ± 0.13
371	8.2	35.13	151	51	0.35 ± 0.01	2.70 ± 0.13	0.57 ± 0.04	2.13 ± 0.13
448	6.8	35.08	180	59	2.21 ± 0.09	1.19 ± 0.16	0.63 ± 0.06	0.56 ± 0.17
599	5.5	35.04	215	69	0.57 ± 0.01	1.92 ± 0.01	0.31 ± 0.02	1.60 ± 0.02
1201	4.2	34.97	247	76	0.35 ± 0.01	1.24 ± 0.04	0.29 ± 0.01	0.96 ± 0.04

2004	3.4	34.94	252	76	0.50 ± 0.01	3.97 ± 0.18	0.76 ± 0.01	3.22 ± 0.18
2602	2.8	34.92	252	75	3.51 ± 0.30	26.02 ± 1.91	0.73 ± 0.02	25.28 ± 1.91
Station B2 (38 14.96 N, 072 45.27 W; St. #10)								
5	24.3	35.25	204	96	2.15 ± 0.05	7.67 ± 0.26	0.47 ± 0.04	7.21 ± 0.26
34	22.8	35.79	238	108	0.30 ± 0.04	6.70 ± 0.15	0.83 ± 0.03	5.87 ± 0.15
95	14.1	35.65	171	67	1.45 ± 0.04	2.07 ± 0.06	0.46 ± 0.06	1.61 ± 0.09
196	12.1	35.52	151	56	0.75 ± 0.02	2.17 ± 0.04	0.50 ± 0.04	1.67 ± 0.05
274	10.0	35.27	130	46	0.42 ± 0.01	1.41 ± 0.09	0.52 ± 0.04	0.89 ± 0.10
449	6.8	35.08	180	59	3.03 ± 0.14	1.41 ± 0.04	0.52 ± 0.02	0.89 ± 0.04

789

Table 2. Columns 2 to 4, the percentage contribution of Mn(III)-L towards total dissolved manganese (dMn_T = manganese(II) + Mn(III)-L_{DFOB}) and oxidized manganese ($_{oxi}Mn$), which is composed of soluble Mn(III)-L_{DFOB} and particulate MnO_x and the ratio (expressed as a percentage) of $_{oxi}Mn$ to dMn_T. Columns 5 to 7, the percentage contribution of each manganese species towards total manganese (Mn_T).

Depth (m)	Mn(III)-L in dMn_T	Mn(III)-L in $_{oxi}Mn$	$_{oxi}Mn / dMn_T$	Mn(II) in Mn_T	Mn(III)-L_{DFOB} in Mn_T	MnO_x in Mn_T
Station A1 (37 07.84 N, 073 19.72 W)						
10	0.2	3.8	4‡	96	0.2	3.8
74	7	20	36	72	6	22
154	3	21	14	87	3	10
225	6	16	39	71	4	25
402	11	43	26	77	10	13
698	7	33	20	82	6	12
Station A2 (37 18.45 N, 073 23.79 W)						
5	0.7	8	9‡	91	1	8
152	5	14	33	74	4	22
256	0.0	0.1	18	85	0	15
325	0.5	5	10	91	1	8
525	5	34	15	86	5	9
825	5	23	22	81	4	15
2032	13	49	27	76	12	12
Station B1 (38 17.40 N, 072 43.70 W)						
11	3	18	17‡	85	3	12
44	6	31	19‡	83	5	12
63	14	36	38	69	11	20
98	20	38	52	61	15	24
194	13	22	60	59	9	32
282	13	24	53	62	9	29
371	21	62	34	70	19	11
448	53	22	238‡	17	18	65
599	16	36	46	64	13	23
1201	23	45	51	60	18	22
2004	19	60	32	72	17	11
2602	3	17	16‡	85	3	12
Station B2 (38 14.96 N, 072 45.27 W)						
10	6	18	34‡	74	4	22
34	12	74	17‡	84	12	4
95	22	24	92	46	13	41
196	23	40	58	57	17	26
274	37	15	67	49	28	23
449	37	55	251‡	20	12	68

‡ External forcings control manganese cycling in these waters; photochemistry in near-surface waters (< 50 m) and nepheloid layer(s) in the bottom water, or these waters had a significant presence of MnO_x indicating a likely presence of microbial manganese oxidizers.

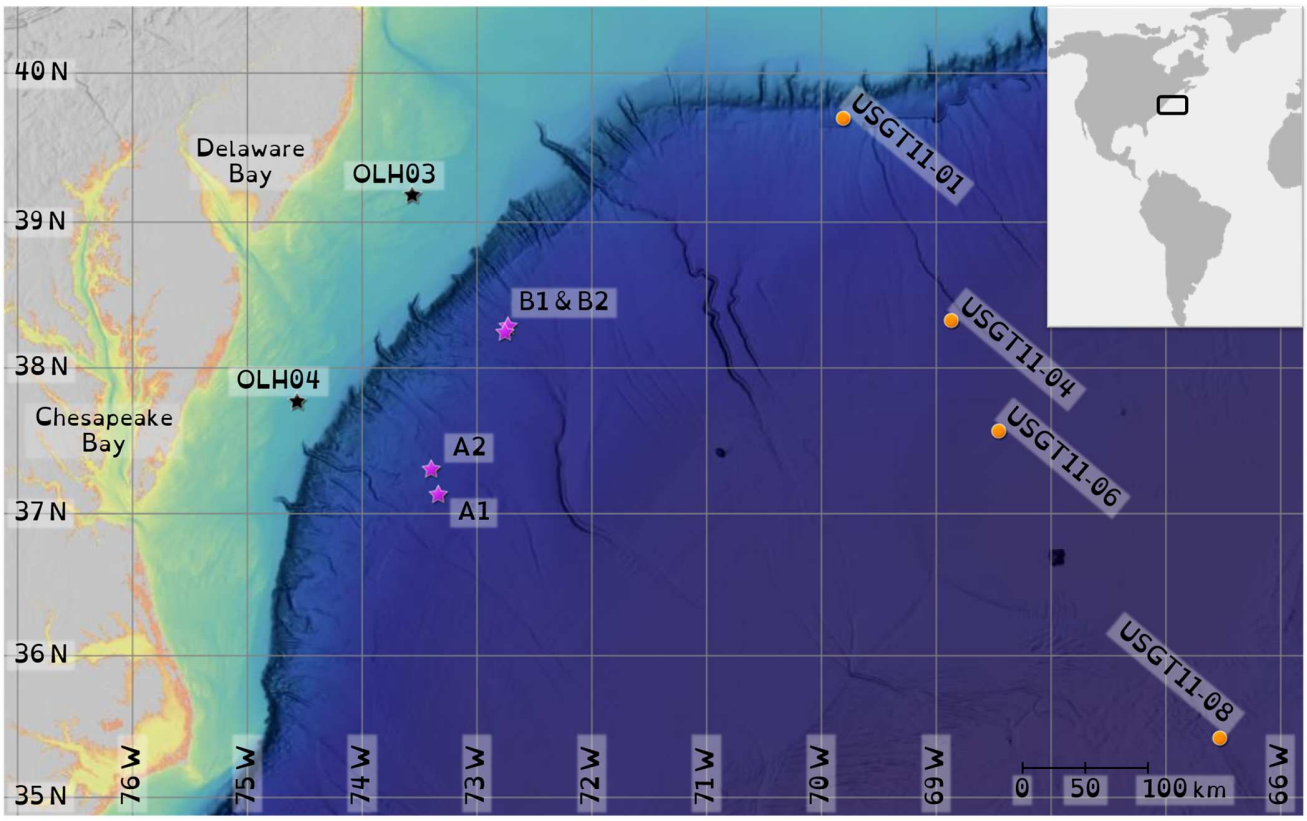

Figure 1. Bathymetry map of the mid-Atlantic Bight (USA east coast) showing sampling station locations for this study (Stations A & B; pink stars) and those referenced in the discussions [GEOTRACES Winter 2011 (USGT11; orange circles), and Oldham et al. (2020) (OLH; black stars)]. Inset, map of North and South America with black rectangle highlighting the sampling region. Station A sampled in August 2013 and Station B in August 2014.

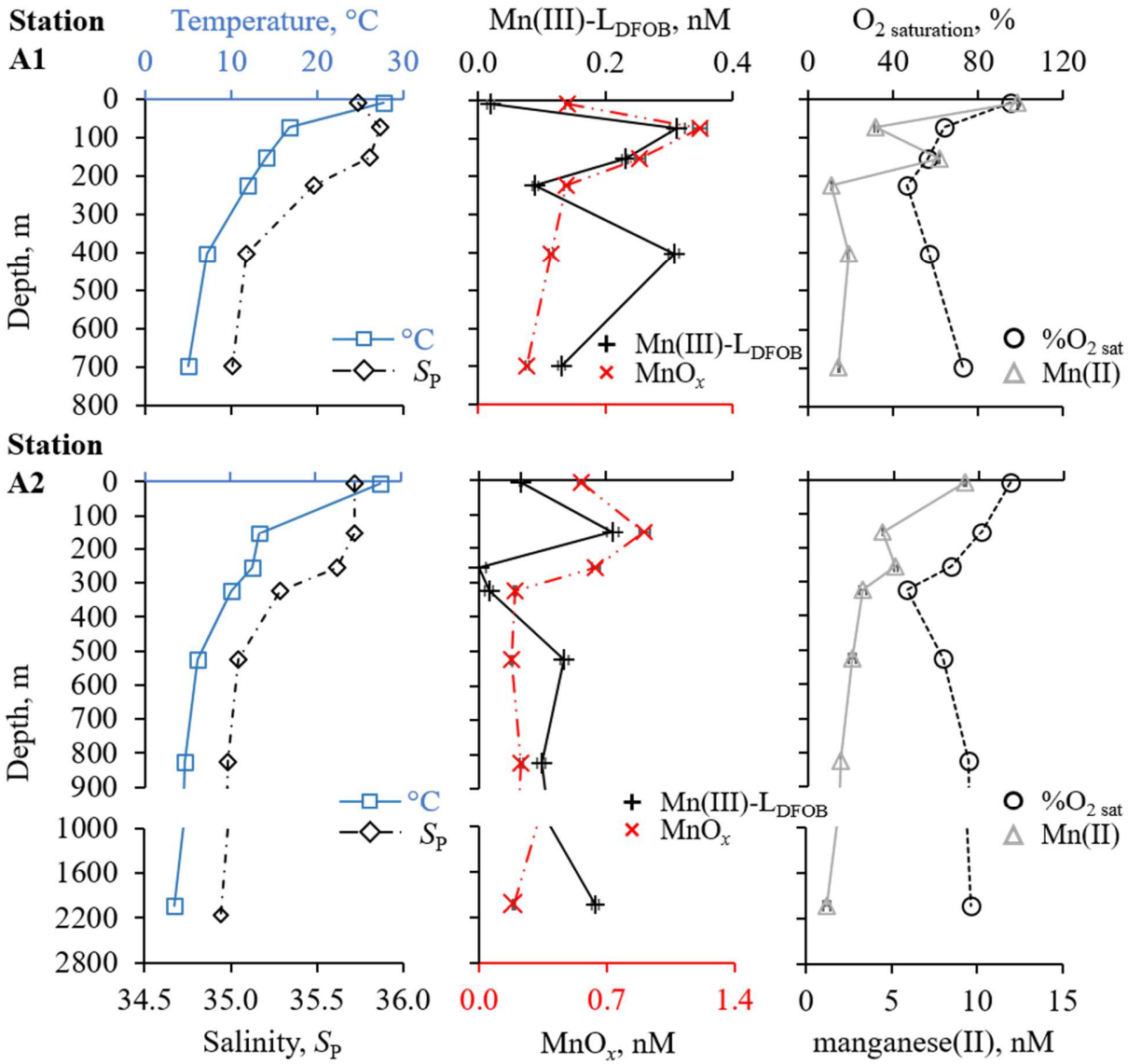

Figure 2. Station A depth profiles for physicochemical parameters and manganese speciation, manganese(II), Mn(III)-L$_{DFOB}$ and MnO$_x$, in Northwest Atlantic offshore waters. The second station (A2) was intended as a repeat profile through that location's oxygen minimum zone.

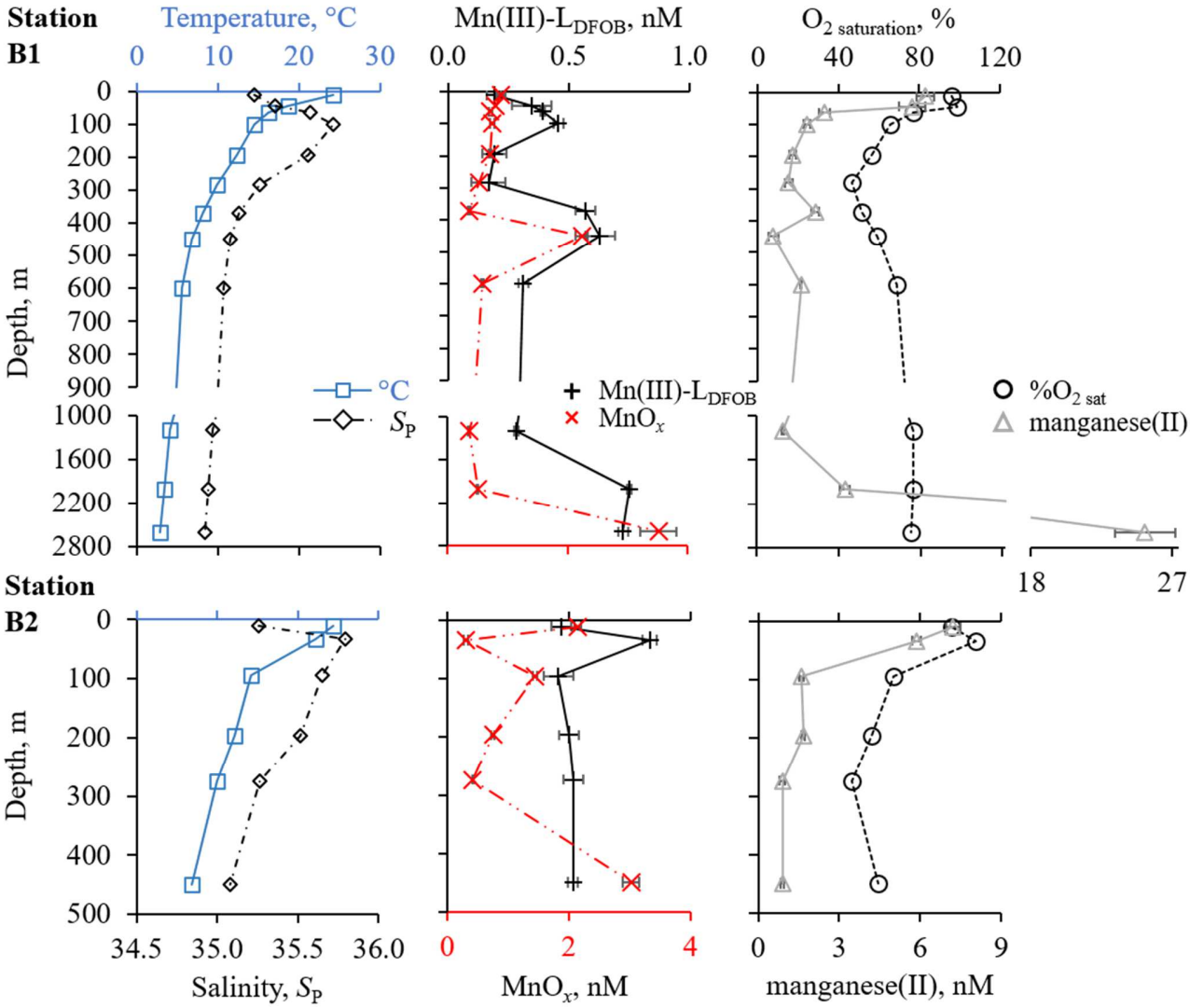

Figure 3. Station B depth profiles for physicochemical parameters and manganese speciation, manganese(II), Mn(III)-L_{DFOB} and MnO_x, in Northwest Atlantic offshore waters. The second station (B2) was intended as a repeat profile through that location's oxygen minimum zone.

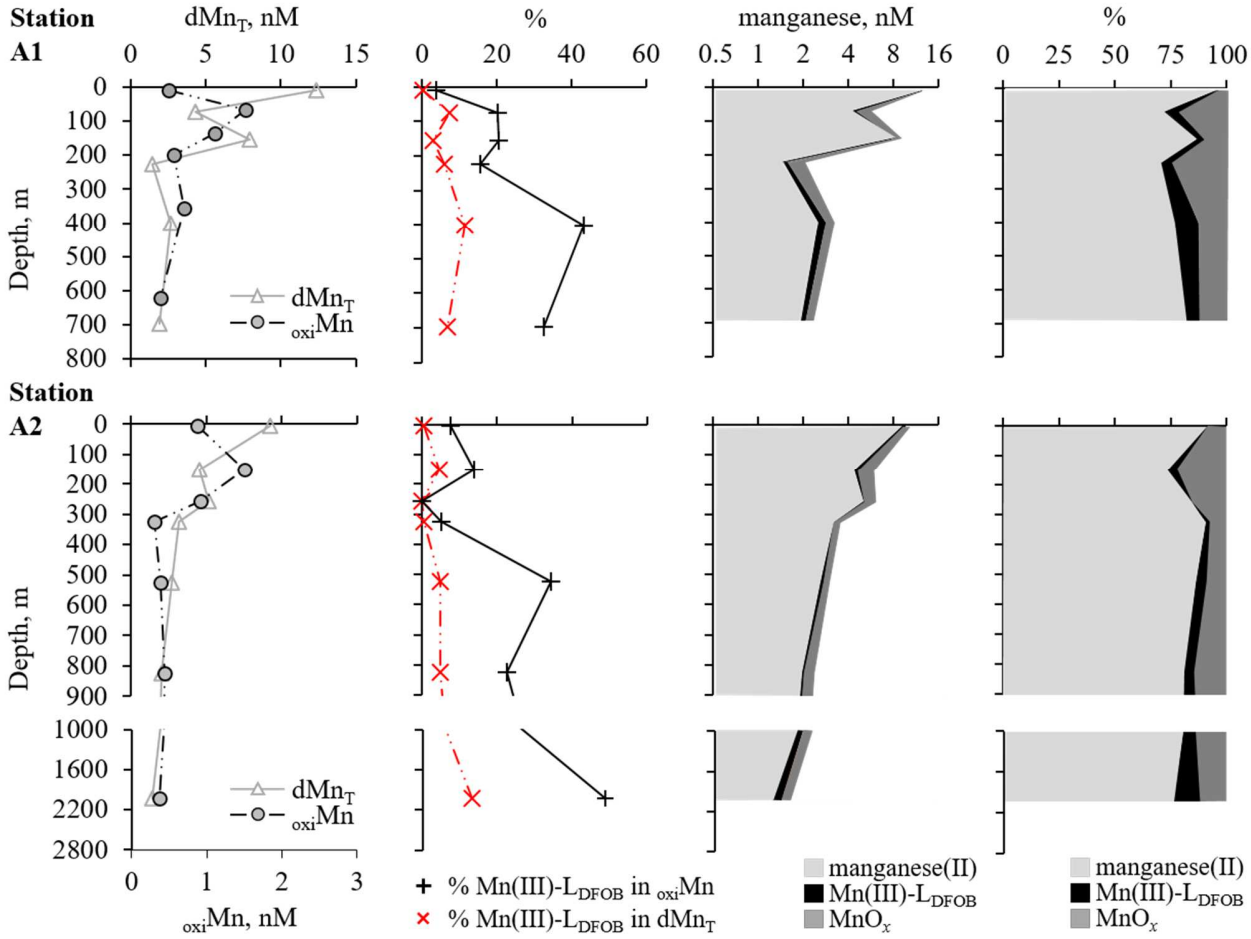

Figure 4. From left to right, 1) Station A depth profiles of the manganese pools, total dissolved manganese (dMn_T = manganese(II) + Mn(III)-L_{DFOB}) and oxidized manganese ($_{oxi}Mn$), composed of soluble Mn(III)-L_{DFOB} and particulate MnO_x. 2) Profiles of the percentage contributions of Mn(III)-L_{DFOB} within $_{oxi}Mn$ and dMn_T (Table 2). 3) Profiles of the contribution of each manganese species to the total bio-available manganese (Mn_T) and 4) profiles of the relative percentage contribution of manganese species within Mn_T in Northwest Atlantic offshore waters (Table 2). Total bio-available manganese concentration (manganese, nM) is presented on a logarithmic (base 2) scale. The second station (A2) was intended as a repeat profile through the oxygen minimum zone.

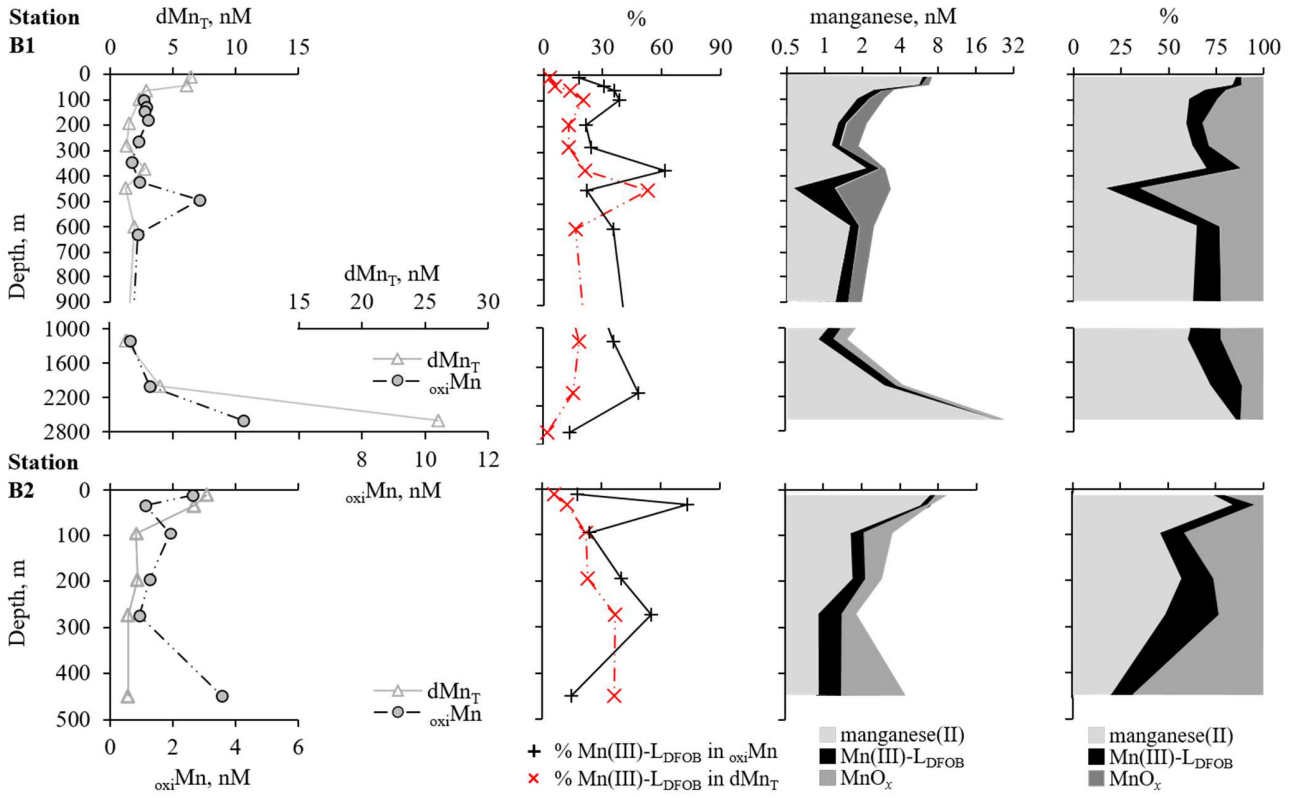

Figure 5. From left to right, 1) Station B depth profiles of the manganese pools, total dissolved manganese (dMn_T = manganese(II) + Mn(III)-L_{DFOB}) and oxidized manganese ($_{oxi}Mn$), composed of soluble Mn(III)-L_{DFOB} and particulate MnO_x. 2) Profiles of the percentage contributions of Mn(III)-L_{DFOB} within $_{oxi}Mn$ and dMn_T (Table 2). 3) Profiles (Table 1) of the contribution of each manganese species to the total bio-available manganese (Mn_T) and 4) profiles of the relative percentage contribution of manganese species within Mn_T in Northwest Atlantic offshore waters (Table 2). Total bio-available manganese concentration (manganese, nM) is presented on a logarithmic (base 2) scale. The second station (B2) was intended as a repeat profile through the oxygen minimum zone.

859

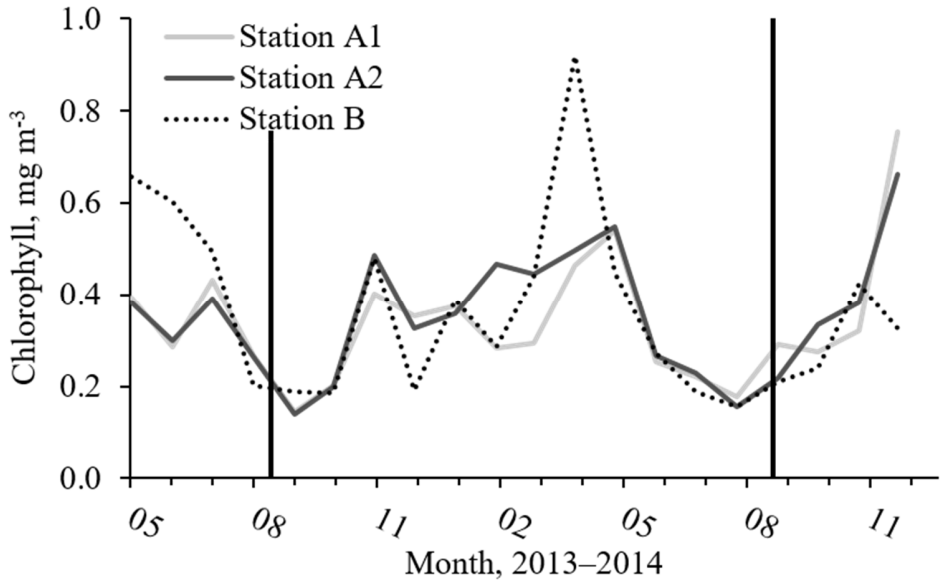

860

861 Figure 6. Mean monthly surface chlorophyll concentrations at Stations A1, A2 and B, taken from
862 National Oceanographic and Atmospheric Administration (NOAA) VIIRS level 3 satellite data. Vertical
863 black lines show occurrence of sampling in August 2013 (Stations A1 and A2) and 2014 (Station B).

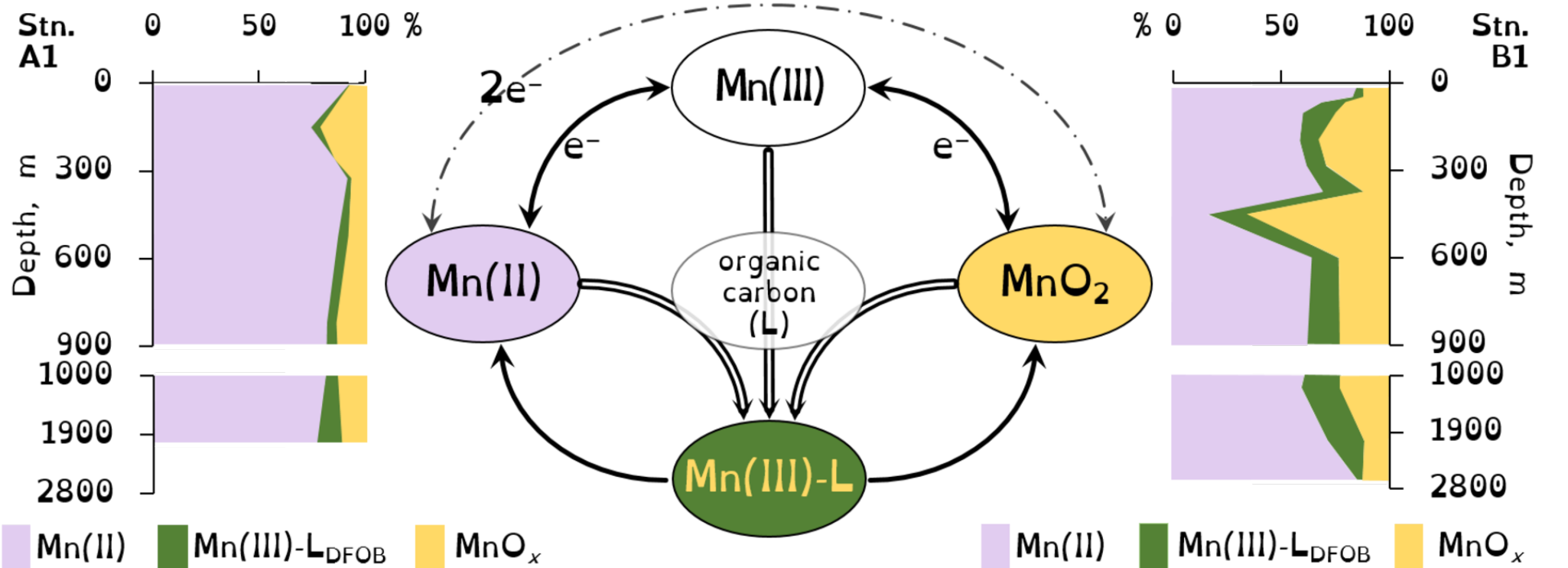
Stn. A1
0
50
100 %
Depth, m
0
300
600
900
1000
1900
2800
2e⁻
e⁻
e⁻
Mn(III)
Mn(II)
organic carbon (L)
MnO2
Mn(III)-L
% 0
50
100
Stn. B1
Mn(II)
Mn(III)-L_DFOB
MnO_x